Mendeleev Communications

Mendeleev Commun., 2026, **36**, 95–97

Oxidation stability of solid-phase ZnS–Ag_2S heteronanostructures

Stanislav I. Sadovnikov* and Aleksandr I. Gusev†

Institute of Solid State Chemistry, Ural Branch of the Russian Academy of Sciences, 620990 Ekaterinburg, Russian Federation. E-mail: sadovnikov@ihim.uran.ru

DOI: 10.71267/mencom.7837

The stability of the phase composition of sulfide heteronanostructures $(ZnS)(Ag_2S)_x$ with $x = 0.025–0.50$ has been investigated for the first time. Annealing of such heteronanostructures in air at temperatures from 298 to 800 K and higher leads to a change in their phase composition due to the oxidation of cubic zinc sulfide to hexagonal zinc oxide. The weight loss that occurs during heating from ~320 to ~700–750 K is associated with the onset of oxidation of zinc sulfide and the formation of zinc oxide.

$(ZnS)(Ag_2S)$ heteronanostructure: ZnS nanoparticles covered by Ag_2S

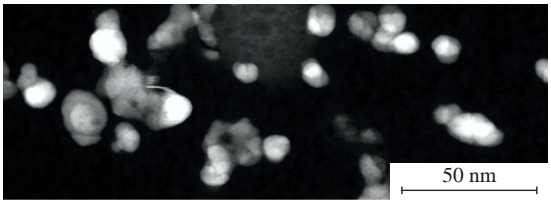

Keywords: chemical co-precipitation, heteronanostructure $(ZnS)(Ag_2S)_x$, composition stability, phase composition, oxidation, silver, zinc sulfide.

Semiconductor sulfides ZnS and Ag_2S are widely used in various electronic devices, solar cells, light-emitting diodes, luminophores and catalysts.[1–5] Cubic (space group $F\bar{4}3m$) zinc sulfide α-ZnS is a wide bandgap semiconductor with a bandgap of $E_g = 3.50–3.76$ eV.[3] Monoclinic (space group $P2_1/c$) silver sulfide (acanthite, α-Ag_2S) exists at temperatures below 450 K. The conventional bandgap of silver sulfide with the α-Ag_2S acanthite structure is 0.9–1.1 eV.[2] In the ideal case, the bandgap of a sulfide heteronanostructure of ZnS and Ag_2S can cover a wide spectral region from infrared to near ultraviolet.

The stability of the phase composition of $(ZnS)(Ag_2S)_x$ heteronanostructures is important for their possible practical application. When heating $(ZnS)(Ag_2S)_x$ heteronanostructures, oxidation of sulfides is possible. The aim of this work was to evaluate the stability of the composition of $(ZnS)(Ag_2S)_x$ heteronanostructures containing different relative amounts of silver sulfide. The compositions of the reaction mixtures and synthesized $(ZnS)(Ag_2S)_x$ heteronanostructures are given in Table 1.

The synthesis of solid-phase $(ZnS)(Ag_2S)_x$ heteronanostructures by the two-stage hydrochemical co-precipitation of ZnS and Ag_2S was described in detail earlier[4] and is presented in Online Supplementary Materials. ZnS–Ag_2S heteronanostructures were synthesized in two stages. First, silver sulfide (Ag_2S) was obtained by chemical precipitation from aqueous solutions of silver nitrate ($AgNO_3$) and sodium sulfide (Na_2S) in the presence of sodium citrate (Na_3Cit). Further, solution of sodium sulfide was added to an aqueous solution of zinc nitrate with constant stirring, and the resulting ZnS solution was mixed with the synthesized colloidal solution of silver sulfide. The synthesis and characterization methods are described in detail in Online Supplementary Materials.

The oxidation of $(ZnS)(Ag_2S)_x$ heteronanostructures with low ($x < 0.025$) silver sulfide content is almost indistinguishable from the oxidation of zinc sulfide. Therefore, this work examines in detail the oxidation stability of four $(ZnS)(Ag_2S)_x$ heteronanostructures with relative silver sulfide content x from 0.025 to 0.50.

The precipitated sulfide powders were examined by X-ray diffraction (XRD) before and after annealing. The final refinement of the structure of the synthesized sulfide heteronanostructures was performed using the X'Pert Plus software package.[6] The evolution of XRD patterns of the $(ZnS)(Ag_2S)_{0.10}$ and $(ZnS)(Ag_2S)_{0.025}$ heteronanostructures with an increase in the annealing temperature in air to 650 K is shown in Figure 1. The quantitative analysis and comparison with published data[7,8] showed that the observed sets of diffraction reflections of the initial heteronanostructures at room temperature (298 K) correspond to single-phase cubic (space group $F\bar{4}3m$) ZnS with a sphalerite structure (type B3). The size of ZnS nanoparticles in the initial heteronanostructure is ~3–4 nm. The lattice constant a_{B3} of ZnS nanoparticles is ~0.5387 nm (see Table 1). An increase in the annealing temperature is accompanied by the intensity growth of diffraction reflections due to an increase in the size of cubic ZnS particles and the appearance of reflections of hexagonal ZnO. The size of ZnS nanoparticles after heating this heteronanostructure in air at 600 and 650 K is ~15–16 and ~18–24 nm, respectively. The XRD pattern of the $(ZnS)(Ag_2S)_{0.10}$ heteronanostructure recorded at room temperature after heating to 650 K also shows diffraction reflections of monoclinic silver sulfide (acanthite, α-Ag_2S). Oxidation of the $(ZnS)(Ag_2S)_{0.025}$ and $(ZnS)(Ag_2S)_{0.10}$ heteronano-

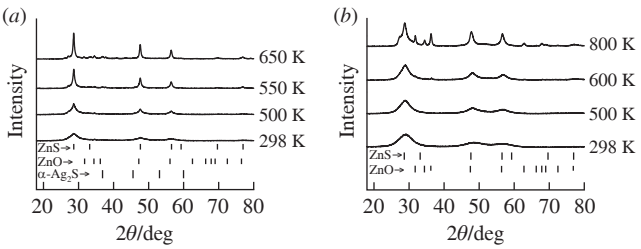

Figure 1 XRD patterns of the initial (298 K) and annealed at different temperatures heteronanostructures (*a*) $(ZnS)(Ag_2S)_{0.10}$ and (*b*) $(ZnS)(Ag_2S)_{0.025}$. The positions of reflections of cubic (space group $F\bar{4}3m$) ZnS, hexagonal (space group $P6_3mc$) ZnO and monoclinic (space group $P2_1/c$) acanthite α-Ag_2S are marked with dashes.

† Deceased.

Table 1 Composition of reaction mixtures, x value and ZnS lattice constant a_{B3} in synthesized $(ZnS)(Ag_2S)_x$ heteronanostructures.

Entry	Concentration (ZnS synthesis)/mmol dm^{-3}		Concentration (Ag_2S synthesis)/mmol dm^{-3}			x value in $(ZnS)(Ag_2S)_x$	a_{B3}/nm
	$Zn(NO_3)_2$	Na_2S	$AgNO_3$	Na_2S	Na_3Cit		
1	50	50	2.5	1.25	0.8	0.025	0.5388
2	50	50	5.0	2.5	2.0	0.05	0.5435
3[a]	50	50	10.0	5.0	4.0	0.10	0.5387
4[a]	50	50	50.0	25.0	10.0	0.50	0.5398

[a] The XRD pattern of the synthesized heteronanostructure showed reflections of monoclinic (space group $P2_1/c$) acanthite α-Ag_2S with lattice parameters $a = 0.4220$, $b = 0.621$, $c = 0.9531$ nm and $\beta = 125.43°$.

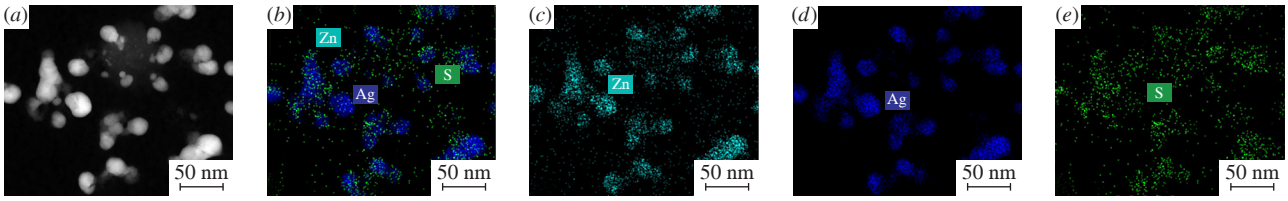

Figure 2 (*a*) HAADF image of the synthesized $(ZnS)(Ag_2S)_{0.50}$ heteronanostructure, (*b*) HAADF-STEM image of this heteronanostructure with overlaid EDX distribution maps of (*c*) Zn, (*d*) Ag and (*e*) S in this heteronanostructure.

structures with the formation of zinc oxide begins at a temperature of ~550 K. The evolution of the XRD patterns of the $(ZnS)(Ag_2S)_{0.05}$ heteronanostructure upon heating in air is the same as for the $(ZnS)(Ag_2S)_{0.025}$ heteronanostructure.

The microstructure of the synthesized ZnS–Ag_2S heteronanostructures was visualized using a transmission electron microscopy (TEM). EDX mapping with almost atomic precision was used to determine the positions of both heavy (Ag, Zn) and light (S) elements. Figure 2 shows the TEM image of the $(ZnS)(Ag_2S)_{0.50}$ heteronanostructure in the HAADF-STEM mode and the distribution of Ag, Zn and S elements in this heteronanostructure. The heteronanostructure is a nanocrystalline matrix of zinc sulfide particles doped with silver sulfide nanoparticles. The content of Ag, Zn and S elements in this heteronanostructure is ~28.5, ~28.5 and ~42.9 at%, respectively. It is evident from Figure 2 that the darker silver-containing Ag_2S nanoparticles with a size of ~3 nm are predominantly located on the surface on the brighter zinc-containing ZnS nanoparticles. According to the XRD data, in the initially synthesized $(ZnS)(Ag_2S)_{0.50}$ heteronanostructure, the size of ZnS and Ag_2S nanoparticles is 6–7 and 3–4 nm, respectively.

Transformations occurring during heating in air and oxidation of the synthesized $(ZnS)(Ag_2S)_x$ heteronanostructures were monitored by differential scanning calorimetry (DSC) and differential thermal analysis (DTA)–differential thermogravimetry in combination with mass spectrometry of the evolved gases. Figure 3 shows, as an example, typical temperature dependences of ion currents (I_{ion}) and a DSC curve measured during heating of the $(ZnS)(Ag_2S)_{0.50}$ heteronanostructure in air to 970 K.

An effect associated with the removal of 3–4 wt% of adsorbed water was observed on the DSC curve at 379 K. Water evaporation is confirmed by the presence of a maximum at ~390 K on the temperature dependence of the ion current for the mass number 18 corresponding to H_2O.[9] When the $(ZnS)(Ag_2S)_{0.50}$ heteronanostructure is heated, the onset of oxidation at 527 K is recorded on the DSC curve. It is manifested in a decrease in the sample mass and the appearance of a small exothermic effect accompanied by the release of SO_2. This can be explained not only by partial sublimation of the formed ZnO, but also by the continuation of ZnS oxidation, which is confirmed by the XRD data. The exothermic effect detected on the DSC curve at ~674 K corresponds to the release of CO_2 due to the oxidation of the citrate carbon-containing radical to carbon dioxide. Previously, it was reported that there is a citrate carbon-containing shell on the surface of heteronanostructures,[4] the oxidation of which is confirmed by a maximum at 661 K on the temperature dependence of the ion current for the mass number 44, corresponding to CO_2 (see Figure 3).

The weight loss occurring upon heating the sample to ~700–720 K is associated with the onset of ZnS oxidation and the formation of ZnO, which has a lower molar mass than ZnS. The largest weight loss of ~12% is observed during heating from ~770 to ~850 K and is due to an increase in the ZnO content and partial oxidation of sulfur, which is removed as gaseous sulfur dioxide (SO_2). The exothermic effect on the DSC curve with a maximum at 857 K correlates with the release of SO_2 into the gas phase and continued oxidation of the heteronanostructure. The release of SO_2 is confirmed by the presence of maxima at ~674 and ~851 K on the temperature dependence of the ion current for the mass number 64 corresponding to SO_2. The partial oxidation of sulfur and its removal in the form of SO_2 were previously observed during the oxidation of silver sulfide[10] and zinc sulfide nanopowders.[11–13]

To conclude, heteronanostructures $(ZnS)(Ag_2S)_x$ with different Ag_2S content were synthesized by the hydrochemical co-precipitation method. The thermal stability of the phase composition of sulfide heteronanostructures $(ZnS)(Ag_2S)_x$ was investigated for the first time. Annealing of the synthesized heteronanostructures $(ZnS)(Ag_2S)_x$ in air at temperatures of 298–800 K and higher is accompanied by the evolution of their phase composition due to the oxidation of cubic zinc sulfide to hexagonal zinc oxide and an increase in the size of ZnS nanoparticles. Oxidation of the heteronanostructures begins at a temperature of 550–600 K, and at an

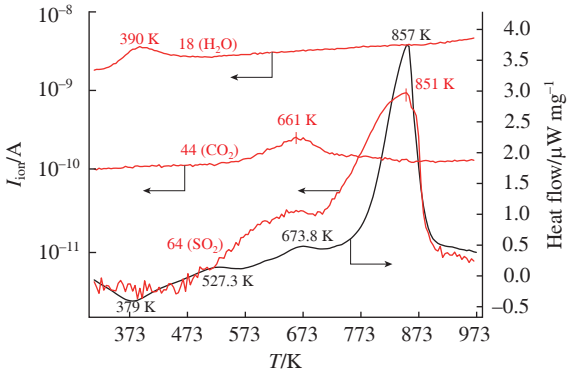

Figure 3 DSC curve measured during heating of the $(ZnS)(Ag_2S)_{0.50}$ heteronanostructure in air and temperature dependences of the ion current (I_{ion}) obtained by mass spectrometric analysis of the evolved gases. The maxima observed at temperatures of ~390, ~661 and ~640–670 K are associated with the release of H_2O vapor and CO_2 and SO_2 gases, respectively.

annealing temperature of ~800 K, the zinc oxide content in heteronanostructures reaches ~26–30 wt%. The size of ZnO nanoparticles depends on the composition of the initial heteronanostructures. At annealing temperatures of 650 and 700 K, it changes from 12 to 17–24 nm and from 13 to 25–30 nm, respectively.

The weight loss observed upon heating to ~390 K is caused by the removal of adsorbed water from the samples, which is confirmed by the presence of a maximum in the temperature dependence of the ion current corresponding to H_2O. Studies of the oxidation of the $(ZnS)(Ag_2S)_x$ heteronanostructures in air have shown that oxidation begins at ~520 K. The largest weight loss of ~12% is observed after heating from ~720 to ~850 K and is due to an increase of the ZnO content, partial oxidation of sulfur and its removal in the form of SO_2. This is confirmed by the presence of maxima at ~674 and ~851 K in the temperature dependence of the ion current corresponding to SO_2.

This work was carried out in accordance with the state assignment FUWF-2024-0010 no. 124020600013-9 for the Institute of Solid State Chemistry of the Ural Branch of the Russian Academy of Sciences. The authors are grateful to Dr. E. Yu. Gerasimov for assistance in the HAADF-STEM study.

Online Supplementary Materials

Supplementary data associated with this article can be found in the online version at doi: 10.71267/mencom.7837.

References

1 X. Fang, T. Zhai, U. K. Gautam, L. Li, L. Wu, Y. Bando and D. Golberg, *Prog. Mater. Sci.*, 2011, **56**, 175; https://doi.org/10.1016/j.pmatsci.2010.10.001.

2 S. I. Sadovnikov and A. I. Gusev, *J. Mater. Chem. A*, 2017, **5**, 17676; https://doi.org/10.1039/C7TA04949H.

3 S. I. Sadovnikov, A. A. Rempel and A. I. Gusev, *Russ. Chem. Rev.*, 2018, **87**, 303; https://doi.org/10.1070/RCR4803.

4 S. I. Sadovnikov, A. V. Ishchenko and I. A. Weinstein, *J. Alloys Compd.*, 2020, **831**, 154846; https://doi.org/10.1016/j.jallcom.2020.154846.

5 C. Liang, K. Terabe, T. Hasegawa and M. Aono, *Nanotechnology*, 2007, **18**, 485202; https://doi.org/10.1088/0957-4484/18/48/485202.

6 *X'Pert HighScore Plus, version 2.2e (2.2.5)*, Malvern Panalytical, 2009; https://www.malvernpanalytical.com/en.

7 R. Sadanaga and S Sueno, *Mineral. J.*, 1967, **5**, 124; https://doi.org/10.2465/minerj1953.5.124.

8 J. T. S. van Aswegen and H. Verleger, *Naturwissenschaften*, 1960, **47**, 131; https://doi.org/10.1007/BF00628510.

9 [dataset] *NIST Chemistry WebBook, NIST Standard Reference Database Number 69,* eds. P. J. Linstrom and W. G. Mallard, National Institute of Standards and Technology, Gaithersburg, MD, 2025; https://doi.org/10.18434/T4D303.

10 D. Živković, M. Sokić, Ž. Živković, D. Manasijević, Lj. Balanović, N. Štrbac, V. Ćosović and B. Boyanov, *J. Therm. Anal. Calorim.*, 2013, **111**, 1173; https://doi.org/10.1007/s10973-012-2300-z.

11 Q.-S. Fu, Y.-Q. Xue, Z.-X. Cui and M.-F. Wang, *J. Nanomater.*, 2014, 856489; https://doi.org/10.1155/2014/856489.

12 A. M. Klyushnikov, S. M. Pikalov and R. I. Gulyaeva, *Chim. Techno Acta*, 2023, **10**, 202310202; https://doi.org/10.15826/chimtech.2023.10.2.02.

13 S. I. Sadovnikov and S. V. Sergeeva, *Russ. J. Inorg. Chem.*, 2023, **68**, 379; https://doi.org/10.1134/S0036023623600120.

Received: 4th June 2025; Com. 25/7837